High Power Laser Science and Engineering, (2025), Vol. 13, e20, 7 pages.
doi:10.1017/hpl.2025.2

HIGH POWER LASER SCIENCE AND ENGINEERING

RESEARCH ARTICLE

Thermal-lens-free active-mirror ytterbium-doped yttrium aluminum garnet amplifier

Grigory Kurnikov[1,2], Mikhail Volkov[1], Anton Gorokhov[1], Ivan Kuznetsov[1], Evgeny Perevezentsev[1], and Ivan Mukhin[1]

[1]*Federal Research Center A.V. Gaponov-Grekhov Institute of Applied Physics, Russian Academy of Sciences, Nizhny Novgorod, Russia*

[2]*Lobachevsky State University of Nizhny Novgorod, Nizhny Novgorod, Russia*

(Received 27 August 2024; revised 27 November 2024; accepted 24 December 2024)

Abstract

A new method is developed for suppressing thermally induced wavefront distortions of the radiation in the active element of disk geometry. The method is based on controlling radial temperature gradients in the active element using a profiled heatsink. An active element with a zero thermal lens developed on the basis of numerical simulation was experimentally demonstrated in a disk laser head. Higher-order phase aberrations in the active element with a profiled heatsink were weaker than in the element with a flat heatsink. Using this method, a thermal-lens-free active-mirror ytterbium-doped yttrium aluminum garnet amplifier with an output energy of 54 mJ at an average pump power of 100 W and a repetition rate of 106 Hz was implemented.

Keywords: disk laser; thermal wavefront distortions; ytterbium laser

1. Introduction

One of the priority tasks in laser engineering today is to increase the average power of pulse periodic lasers. A serious problem to be solved is thermally induced effects arising in the active elements (AEs). An increase in the absolute temperature in active media leads to deterioration of the spectroscopic characteristics of ytterbium materials[1–3]. An increase in the temperature gradients causes distortions of the polarization and wavefront[4,5] of the laser signal, as well as mechanical stresses in the AE that can destroy it (thermal shock). The use of a thin-disk AE enables effective heat removal. Signal gain, on the other hand, is reduced (e.g., due to amplified spontaneous emission (ASE) becoming more evident) and the consequent thermally induced deformations of the AE appear to be significant. Since multipass amplification schemes should be used in such AEs, radiation wavefront distortions (over all passes) remain significant, despite the effective cooling of the disk AE. The resulting thermally induced wavefront distortions may be reduced by controlling the distribution of heat sources, as was done in Ref. [6]. One of the cited authors, Ken-ichi Ueda, also proposed to control heat removal from the AE to suppress the negative effects associated with dn/dT[7]. A method for controlling heat flows in disk AEs by profiling the surface of the cooling heatsink was described in Ref. [8], where the results of suppressing the thermal lens and accompanying thermally induced radiation distortions in composite disk AEs were also reported.

The second section of this work is devoted to optimizing the design of the heatsink, taking into account the ideas proposed in Ref. [8], with the aim to effectively cool the ytterbium-doped yttrium aluminum garnet (Yb:YAG) disk AE, with complete suppression of the parabolic component of the thermal lens and reduction of higher-order phase distortions. In the third section of the work, the efficiency of suppression of wavefront distortions is confirmed experimentally. Efficient amplification of laser pulses in a multipass disk amplifier under the conditions of complete suppression of the thermally induced lens is demonstrated in the fourth part of the paper.

2. Optimization of disk active element cooling

The main idea of suppressing radiation wavefront distortions is the correct choice of the heat resistance profile at the border of the AE at a given heat source distribution[8].

Correspondence to: M. Volkov, Federal Research Center A.V. Gaponov-Grekhov Institute of Applied Physics, Russian Academy of Sciences, Nizhny Novgorod 603950, Russia. Email: pine@ipfran.ru

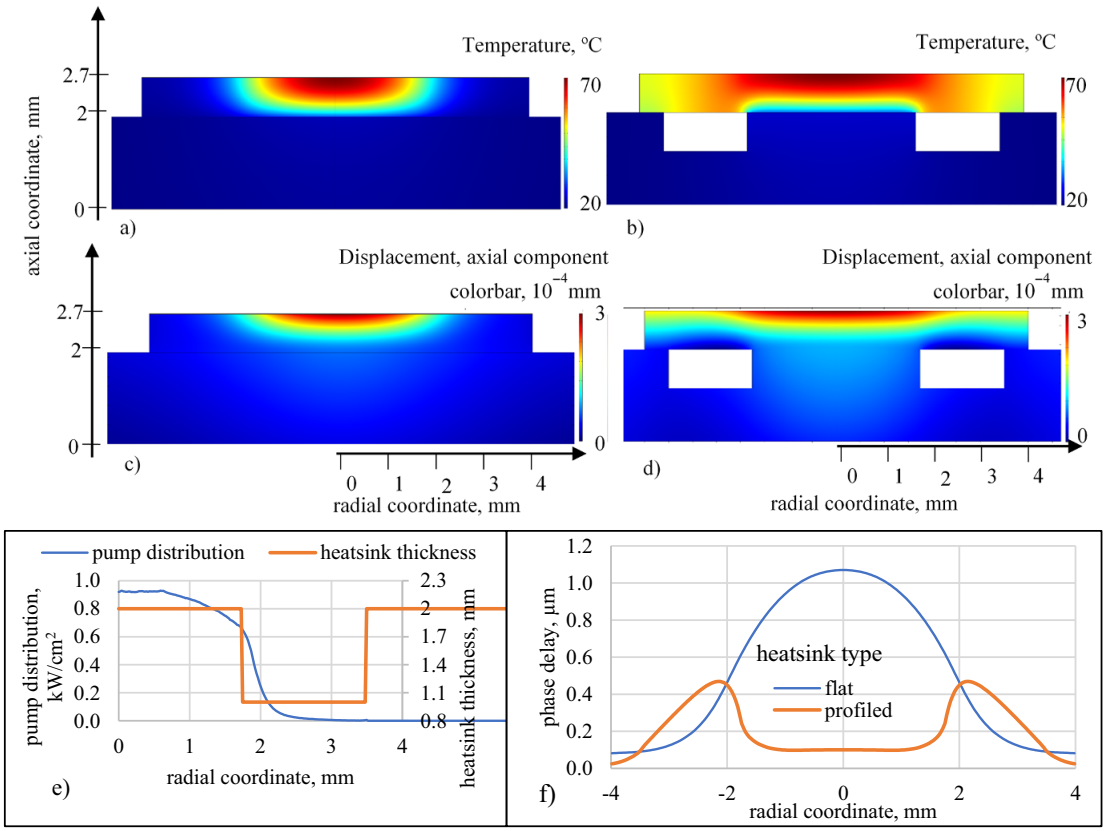

Figure 1. (a), (b) Calculated temperature distributions and (c), (d) axial displacement fields corresponding to AE on flat (a), (c) and profiled (b), (d) heatsinks at absorbed pump power of 100 W and element thickness of 800 μm. (e) Pump and heatsink profile for calculations. (f) Calculated change of the optical path corresponding to geometries (a) and (c) at 100 W pump power.

The profiled heatsink (Figures 1(b) and 1(c)) provides a high heat transfer coefficient inside a circular area corresponding to the pump spot, as well as at the AE periphery. Part of the AE has no direct contact with the heatsink. Only the part of the AE where the sources of heat are located ensures thermal contact. In the central area they are due to pump light absorption and quantum defects and at the periphery to luminescence absorption on the side surface. This heatsink profile minimizes radial heat flows in the AE, unlike the flat one depicted in Figures 1(a) and 1(c). To quantify the required heatsink profile, as well as its impact on temperature and wavefront distortions, the temperature and strains in an Yb:YAG AE with a diameter of 8 mm, a thickness of 800 μm and a doping of 5% (atomic fraction) were calculated. A heatsink with the diameter of 20 mm and the thickness of 1.9 mm was fabricated. The AE geometry and doping were chosen so as to optimize the amplification of laser pulses with pumping at a reduced duty cycle. Similar to Ref. [8], the calculations were based on the equations of thermal conductivity and elasticity, taking into account the experimentally measured coefficient of heat transfer between the AE and the heatsink of 8.7 W/(cm^2 K). The transverse distribution of the laser diode pump shown in Figure 1(c) was used in the model. The resulting temperature distribution (Figures 1(a) and 1(b)), axial displacement (Figures 1(c) and 1(d)) and signal wavefront distortions (Figure 1(f)) at a pump power of 100 W demonstrated that the radial temperature gradients in the AE on a profiled heatsink were smaller than on a flat one; the phase distribution in the operating region was flat, and there was only a slight difference between the maximum temperature readings.

3. Measurement of thermally induced wavefront distortions of radiation in a disk active element

The above idea of minimizing the thermal lens was implemented in the experimental disk laser head[9] (Figure 2(c)). The experimental setup with a pump power variable within 100 W provided water cooling of the heatsink and eight passes of pump radiation through the AE. To record phase distortions, the setup was supplemented with a Michelson interferometer (Figure 2(c)). The AE and the heatsinks (Figure 2(b)) were the same as the ones calculated in the previous section. One heatsink had a flat profile, while the other had a groove. According to the preliminary calculations, the diameter of the central plateau of the profiled heatsink was 3.5 mm, while the outer diameter of the groove was 7 mm (Figure 2(a)).

https://doi.org/10.1017/hpl.2025.2 Published online by Cambridge University Press

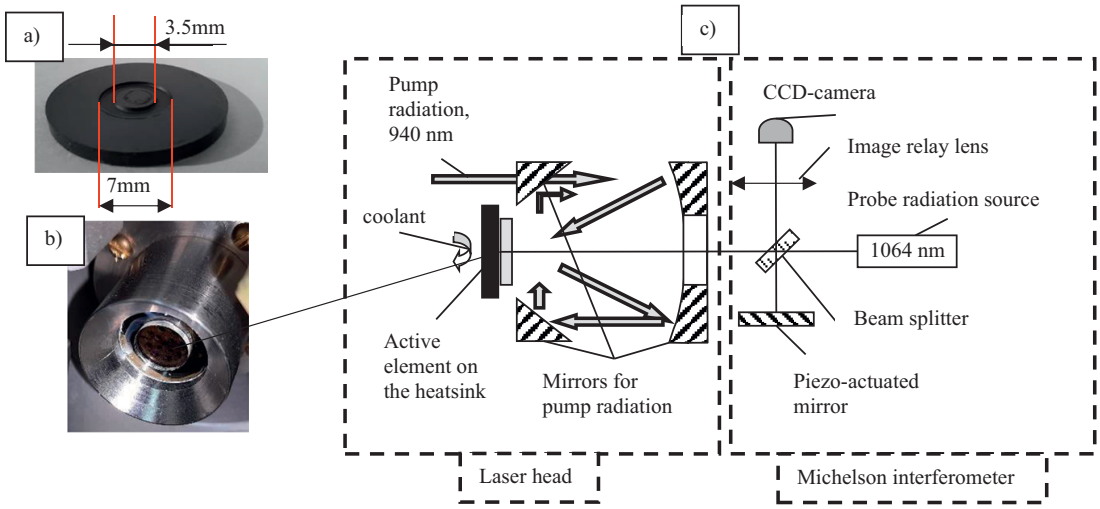

Figure 2. (a) Photo of the profiled heatsink, (b) the active element and heatsink in the holder and (c) diagram of the experimental setup for measuring signal wavefront distortions in the active element under pumping. The scheme includes a system for pumping and cooling of the active element (laser head), as well as a Michelson interferometer for phase-shift interferometry.

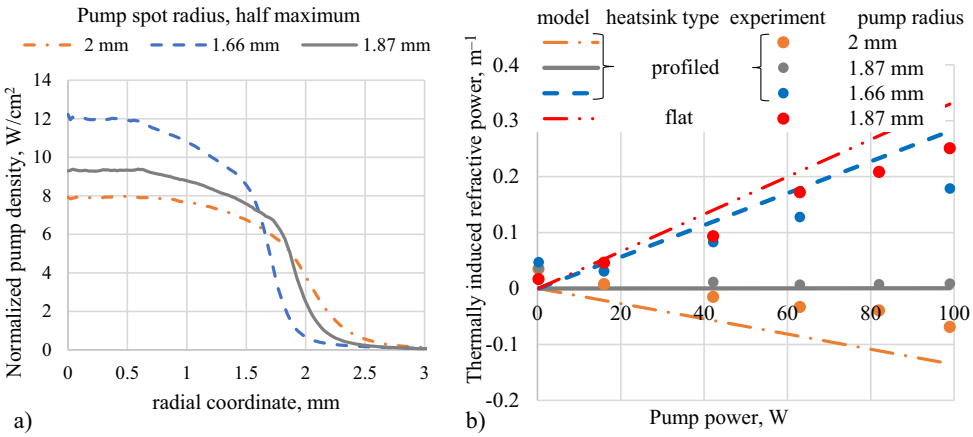

Figure 3. (a) Radial distribution of the pump profile in the active element, three variants of different sizes, obtained during the experiment. The curves indicate the dependence of power density on the radial coordinate, where the colors correspond to different sizes and the graphs are normalized to 1 W. (b) Measured dependence of the thermal lens on pump power corresponding to different sizes of the pump spot with profiled and flat heatsinks.

The transverse pump distribution is shown in Figure 3(a). Figure 4 presents two-dimensional distributions of wavefront distortions in the AEs mounted on the flat and profiled heatsinks at pump powers of 0 and 100 W. These distributions were approximated by a quadratic function of coordinates inside a circle with a diameter of 3.3 mm (shown in Figure 4). The magnitude of the parabolic component of the thermally induced distortions was calculated as the sum of two highest-order coefficients of quadratic fit. A series of numerical simulations and fitting some experimental data led to defining the pump spot size (Figure 3(a), 1.87 mm) at which the parabolic component of the thermally induced distortions was minimal (comparable to the experimental error). For the pump diameter of the same size, the AE on the flat heatsink demonstrated positive thermal lensing that, as indicated by the numerical calculation, could not be suppressed by varying the pump diameter. The resulting lens powers are plotted in Figure 3(b).

Figure 3 expressly shows that by optimizing the heatsink profile as well as the size of the pump spot one can indeed reduce the parabolic component of the wavefront distortion in the disk AE under consideration to zero. However, higher-order aberrations may still persist in the AE, resulting in degraded output beam quality. These aberrations are composed of two components: the so-called built-in (cold) components of phase distortions shown in Figures 4(a) and 4(c), and the thermally induced ones shown in Figures 4(b) and 4(d). The built-in part of the distortions is determined by a deviation of the AE surface from a perfect flat one during its manufacture and mounting on the heatsink. The procedure of manufacture of the AEs for disk laser heads is beyond the scope of this work. Therefore, here we consider only the thermally induced part of the aberrations and their influence on the radiation quality. The aberration magnitude is calculated as the difference between the wavefront retardation at maximum and zero pumping, after which the quadratic

https://doi.org/10.1017/hpl.2025.2 Published online by Cambridge University Press

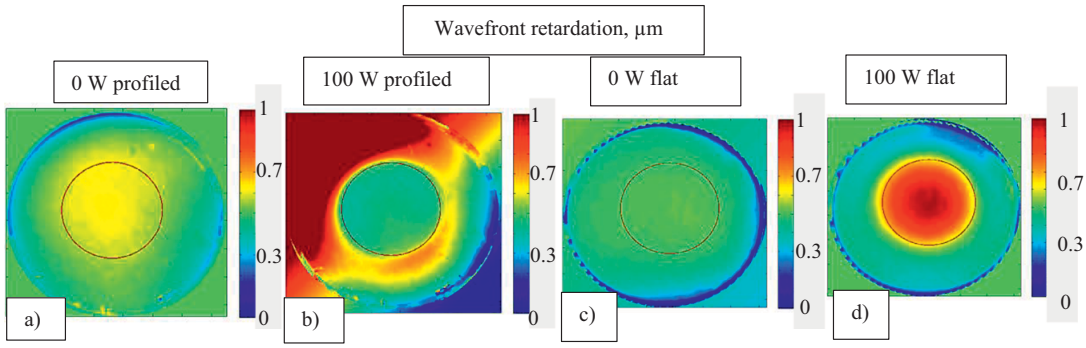

Figure 4. Two-dimensional distribution of wavefront distortions in the AE, pump size 1.87 mm full width at half maximum (FWHM): (a), (b) on a profiled heatsink at 0 and 100 W pump power; (c), (d) on a flat heatsink. The red circle marks the area within which the approximation is made. The diameter of the red circle is 3.3 mm, while the diameter of the entire depicted area is 6.6 mm; the color scale is in micrometers.

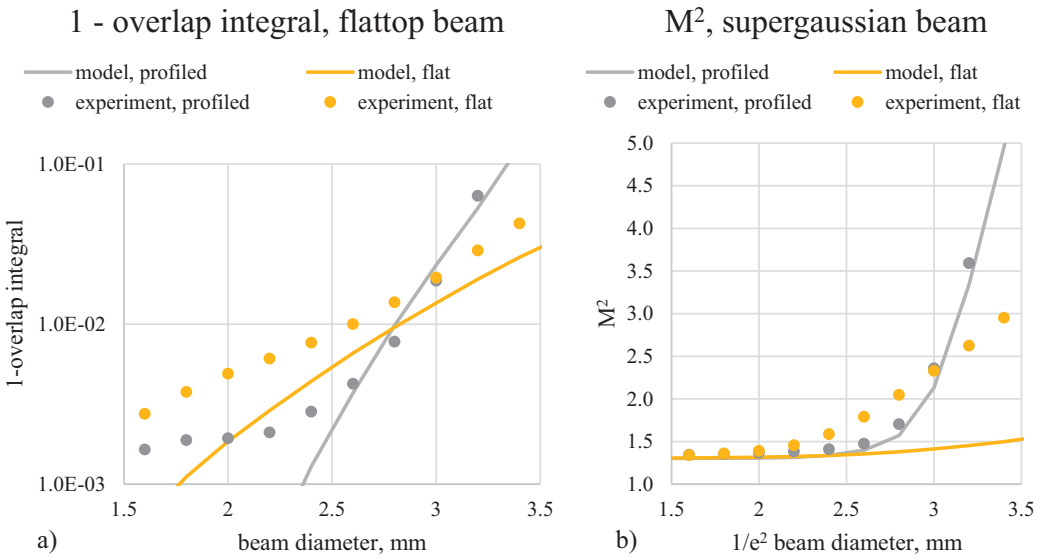

Figure 5. The influence of thermally induced wavefront distortions on probe beam quality: (a) deviation of the overlap integral from unity; (b) value of M^2. The diameter of the probe beam is plotted along the abscissa. 'Experiment' means that the distortion has been measured and the presented value is calculated based on this; 'model' means that both the distortion and the presented value have been calculated.

(parabolic) component is subtracted from the obtained result, since the latter does not affect beam quality. The two-dimensional phase distributions $\varphi(x,y)$ calculated in this way are further used to assess the quality of the laser beam. The calculations are made assuming that the beam with known distribution of the electric field and initial flat wavefront acquires the phase distortions $5\varphi(x,y)$ calculated above. The factor of 5 corresponds to the laser beam propagation in a five-pass amplifier with image relay for each pass as, for example, in Ref. [10]. We evaluate the laser beam quality by two quantities: the overlap integral χ[11] and the parameter M^2[12]. The overlap integral χ is calculated as follows:

$$\chi = \frac{\left|\iint_{\Omega} E_{\text{in}} E_{\text{out}} \mathrm{d}S\right|^2}{\iint_{\Omega} |E_{\text{in}}|^2 \mathrm{d}S \iint_{\Omega} |E_{\text{out}}|^2 \mathrm{d}S} = \frac{\left|\iint_{\Omega} \exp\left(i5\varphi\left(x,y\right)\right)\, \mathrm{d}S\right|^2}{\Omega^2}. \quad (1)$$

Here, E_{in} is the electric field of the beam with allowance for the phase before passing through the aberration element, while E_{out} is after. The calculations by Equation (1) were made assuming that the incident beam had a uniform distribution of electric field strength in the circular region Ω; outside this region the field was zero (flattop beam); the aberrating element introduces only the phase distortions $5\varphi(x,y)$, without changing the intensity distribution; Ω simultaneously denotes the domain of integration and its area. The overlap integral determined in this way was calculated for different diameters of the flattop beam, given that the parabolic part of the distortion was equal to zero at each specific diameter. Since χ differed little from unity, the value presented in Figure 5(a) is $1-\chi$.

The value of M^2 is calculated for a particular beam, depending on its size in the waist and divergence in the far field according to the following formula:

$$M^2 = \frac{2\pi}{\lambda}\sigma_0\theta;$$
$$\sigma^2(z) = \frac{\iint I(x,y,z)\left(x^2+y^2\right)\mathrm{d}x\mathrm{d}y}{\iint I(x,y,z)\,\mathrm{d}x\mathrm{d}y} = \sigma_0^2 + \theta^2 z^2;$$
$$\iint I(x,y,z)\left(\overrightarrow{x_0}x + \overrightarrow{y_0}y\right)\mathrm{d}x\mathrm{d}y \overset{\text{def}}{=} 0. \quad (2)$$

https://doi.org/10.1017/hpl.2025.2 Published online by Cambridge University Press

Here, λ is the radiation wavelength, σ_0 is the beam radius in the waist, θ is the half divergence angle in the far field, $\sigma^2(z)$ is the square of the second moment of the beam, $I(x,y,z)$ is the beam intensity distribution, x, y, z are the Cartesian coordinates and $\overrightarrow{x_0}$, $\overrightarrow{y_0}$ are the unit vectors along the corresponding coordinates; the z-axis is chosen along the direction of beam propagation, that is, the first moment of beam intensity along this axis is zero. It should be noted that no direct experiments were taken to calculate the M^2 criterion. Instead the Fresnel software developed at the A.M. Prokhorov General Physics Institute of the Russian Academy of Sciences was used. Thus, it was possible to simulate the propagation of a light beam with arbitrary distribution of electric field strength and arbitrary wavefront distortions, and also to calculate the beam quality criterion using Equation (2). A beam with intensity distribution described by a super-Gaussian function of the third degree was taken to be the initial beam in our model. This intensity distribution with a flat (unperturbed) wavefront has the criterion $M^2 = 1.303$. The wavefront distortions $\varphi(x,y)$ calculated above and the radiation wavelength of 1030 nm were adopted in the model. The beam acquired phase aberrations equal to $5\varphi(x,y)$, which corresponds to the laser beam propagation in a five-pass amplifier with image relay for each pass as, for example, in Ref. [10]. Next, the value of M^2 was calculated. This procedure was performed for beam diameters from 1 to 4 mm at the $1/e^2$ level; the result is given in Figure 5(b). The results presented in Figures 5(a) and 5(b) indicate that in a certain range of beam diameters, the AE on the profiled heatsink affected the beam quality less than the AE on the flat one. In our case, this interval had an upper limit of 3 mm. The upper limit of the interval was 85% of the diameter of the heatsink contact plateau (which was 3.5 mm), and 75% of the diameter of the pump spot at the $1/e^2$ level (Figure 3(a), curve with legend 1.87 mm). This relationship is valid from the point of view of both criteria: M^2 and the overlap integral. The upper limit for the signal beam size also implies a certain limit for energy extraction efficiency. However, in other works[5,13,14] the signal beam size does not exceed 0.8 of the pump size although the disk is mounted on a flat heatsink. It should be remembered that the presented calculation was performed only taking into account the thermally induced part of the distortion.

4. Multipass disk amplifier with a zero thermal lens

The main problem of thin-disk AEs is low gain per pass. To increase the efficiency of energy extraction from such AEs, amplifiers with several passes of radiation through the medium are used[10,15–18]. However, the AE adds distortions to the beam at each pass, resulting in a significant change in the beam diameter in the optical elements. Telescopic multipass amplifiers taking into account the thermally induced lens in the AE that may be compensated at each pass were proposed in Ref. [19]. However, this approach works only for a constant lens that does not depend on pump power. This limits both the operating and adjustment modes to a specific average heat release power. Basically it is the maximum pump power mode that is of the utmost interest, but in this case the scheme is hardly adjustable. In this regard, the use of the above mechanisms for thermal lens suppression in AEs is highly promising in present-day laser engineering. This section is devoted to the development of a thermal-lens-free multipass Yb:YAG disk amplifier with high average power (Figure 6(a)) based on the laser head shown in Figure 2(c) and the attained results. Radiation from the master oscillator was fed into the amplifier above the spherical mirror onto a flat mirror FM1. Next, using a telescope consisting of a spherical mirror (SM) and a focusing lens (Lens), the image of the radiation from mirror FM1 was transferred to the AE. A flat mirror FM2 was required for beam folding. After reflection from the AE, the image was transferred back to the flat mirror. In this way, five V-passes of radiation were implemented through the disk AE and the radiation output was organized above the spherical mirror. The diameter of the signal radiation beam at the $1/e^2$ level was 3.2 mm, the pulse energy was 2.23 mJ with a duration of 5 ns and the repetition rate was 106 Hz. A diode laser (BWT Beijing) was used for pumping at a central wavelength of 969 nm, a maximum power of 1000 W and a flattop transverse profile (Figure 6(c)). The diameter of the pump spot on the AE approximately corresponded to the diameter of the central plateau on the heatsink equal to 3.5 mm. The pump radiation was modulated with the frequency of the seed signal; the duration of the pump pulse was 1.2 ms. The pulse energy at the output of the scheme as a function of the pump energy is plotted in Figure 6(b). The maximum achieved energy at the amplifier output was 54 mJ, the total gain was a factor of 9.3 and the gain per V-pass was 1.55. At small signal gain (no saturation), the gain per V-pass was 1.67. In the absence of pumping, $M^2 = 1.16$, averaged over two axes. At maximum energy, M^2 of the output signal slightly increased (to 1.44), which is a good result considering the super-Gaussian shape of the pulses.

Using an infrared conversion viewer and a charge-coupled device (CCD) camera, we did not visually detect any changes in the diameters of laser beams on optical elements with increasing pump power, which greatly simplified work with this amplifier. Precision measurements of the thermal lens were made in two ways. The first one was by means of a Michelson interferometer, as described above. The resulting dependence of the thermal lens averaged over two axes on the average absorbed pump power is plotted in Figure 7. As is evident, the values fluctuate within the measurement error. A typical thermal load on the AE was 1.5 times lower compared to the experiments described in the previous section (Figure 3), since pumping was made at a wavelength

https://doi.org/10.1017/hpl.2025.2 Published online by Cambridge University Press

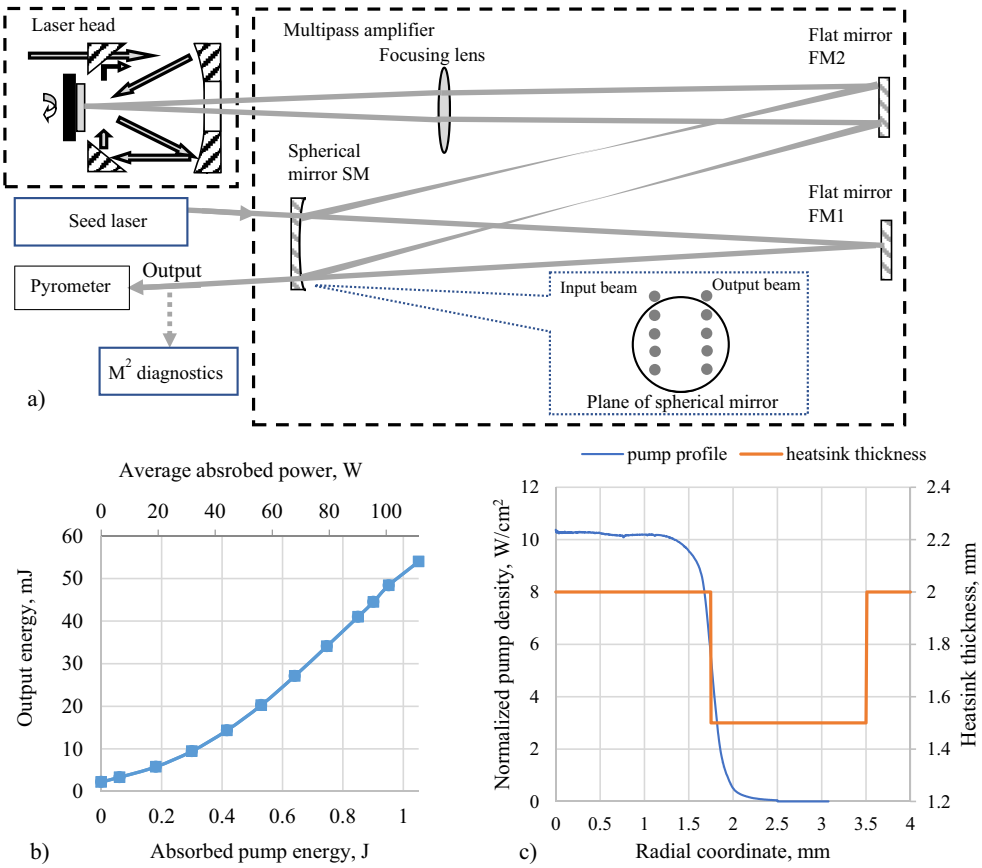

Figure 6. (a) Layout of the laser amplifier with the disk AE, including the laser head with pump injection system and cooling, and a multipass signal amplification scheme. (b) Output pulse energy versus pump pulse energy. (c) Pump density distribution along the radial coordinate, and the heatsink profile used in this amplification scheme.

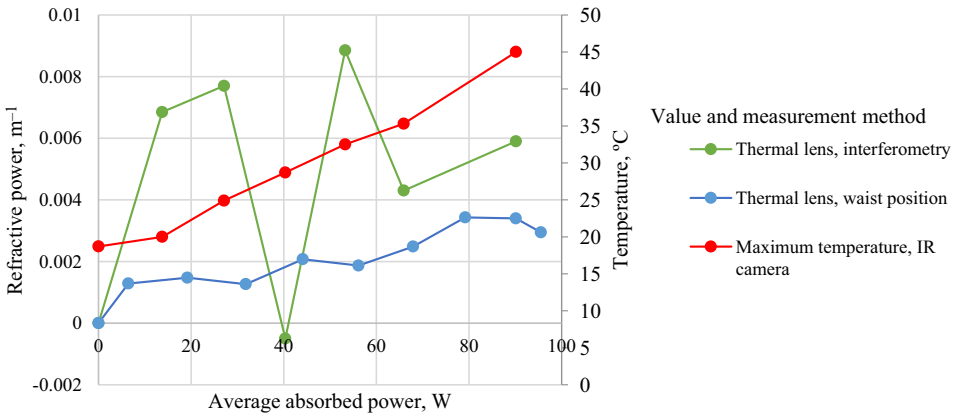

Figure 7. Thermal lens strength and temperature of the AE surface versus average pump power. The lens strength was measured by two methods.

of 969 nm (zero phonon line). To estimate the amount of AE heating, it is necessary to consider the dependence of the AE surface temperature on the pump power (Figure 7).

The other method of thermal lens measurements in the amplifier was using the Ophir BeamSquared system, which accurately determined the waist position after the focusing lens and, hence, the signal divergence. The radiation from the AE was directed to the BeamSquared lens with a focal length of 406.78 mm by means of a long-focus telescope with a magnification factor of 3.4. In the absence of pumping, the radiation was focused 409.2 mm past the lens. A small signal divergence could be caused by both a cold lens in the AE and an error in the telescope adjustment. With an increase in the average pump power to 100 W, the distance between

https://doi.org/10.1017/hpl.2025.2 Published online by Cambridge University Press

the waist and the focusing lens increased to 410.2 mm, which, taking into account the magnification coefficient in the telescope and the image relay from the AE, is equivalent to a lens in the AE of approximately 50 m. It should be noted that this is the case of a lens formed in five passes through the AE; therefore, the lens per reflection in the AE has a focal length of approximately 250 m. The dependence of the thermal lens averaged over two axes in the AE on the average absorbed pump power is shown in Figure 7. It is clear that the obtained values were negligible in the implemented laser amplifier, and lower than the error value of the interferometric measurement method.

5. Conclusion

The method of complete suppression of the thermal lens in an AE of active-mirror geometry under the conditions of strong thermal load has been proposed and experimentally implemented for the first time. The method involves the use of a profiled heatsink plate and accurate fitting of the pump spot diameter. It has been experimentally shown that the parabolic part of wavefront distortions (thermally induced lens) is reduced to zero with this method. Analysis of the performed calculations and of the experimental data has demonstrated a possibility to reduce higher-order phase distortions, provided that the signal beam size is less than 85% of the central plateau of the heatsink and less than 75% of the pump spot at the $1/e^2$ level. An important advantage is the maintained efficient cooling of the active region.

The demonstrated results were achieved for a relatively large thickness of the disk AE optimal for amplification using quasi-continuous-wave pumping. It should be noted that this method of suppressing thermally induced phase distortions allows the use of AEs with any available aperture and thickness, including thin-disk AEs with continuous pumping, which will require additional optimization of the heatsink profile. The use of composite disk AEs provides an alternative application of this approach under continuous pumping , as is demonstrated in Ref. [8].

Based on the proposed method of suppressing the thermal lens in the AE, a thermal-lens-free multipass Yb:YAG disk amplifier with high average power was developed. An average gain per V-pass by a factor of 1.55 with a maximum energy at the amplifier output of 54 mJ was obtained using diode pumping with a peak power of 1000 W. At maximum pump power, M^2 was 1.44 and the average thermal lens in the AE per reflection, measured using BeamSquared, was approximately 250 m. The high potential of the approach to the development of high average power systems based on the thermal lens suppression method described above is further substantiated by the high gain of the demonstrated amplifier while the thermal lens and M^2 values are consistently small.

Acknowledgements

The research was supported by the State Research Task for the Institute of Applied Physics, Russian Academy of Sciences (Project No. FFUF-2024-0043) and by the scientific program of the National Center for Physics and Mathematics (project ‘Physics of High Energy Densities. Stage 2023–2025’).

The authors thank Prof. Ken-ichi Ueda for use of his idea of controlling the heat flows in the AE.

References

1. D. C. Brown, R. L. Cone, Y. Sun, and R. W. Equall, IEEE J. Sel. Top. Quantum Electron. **11**, 604 (2005).
2. J. Dong, M. Bass, Y. Mao, P. Deng, and F. Gan, J. Opt. Soc. Am. B **20**, 1975 (2003).
3. D. S. Sumida and T. Y. Fan, in *Advanced Solid-State Lasers* (1994), paper YL4.
4. A. V. Mezenov, L. N. Soms, and A. I. Stepanov, *Thermooptics of Solid-State Lasers Mechanical Engineering* (Leningrad, 1986), p. 199.
5. J. Mende, E. Schmid, J. Speiser, G. Spindler, and A. Giesen, Proc. SPIE **7193**, 71931V (2009).
6. J. Song, A. Liu, K. Okino, and K.-I. Ueda, Appl. Opt. **36**, 8051 (1997).
7. K.-i. Ueda, in *4th International Symposium on High Power Laser Science and Engineering* (2021).
8. M. Volkov, I. Kuznetsov, G. Kurnikov, and I. Mukhin, Opt. Contin. **2**, 473 (2023).
9. M. R. Volkov, I. Kuznetsov, I. B. Mukhin, and O. V. Palashov, Quantum Electron. **49**, 354 (2019).
10. A. M. Scott, G. Cook, and A. P. G. Davies, Appl. Opt. **40**, 2461 (2001).
11. E. Perevezentsev, A. Poteomkin, and E. A. Khazanov, Appl. Opt. **46**, 774 (2007).
12. A. E. Siegman, Proc. SPIE **1224**, 13 (1990).
13. T. Dietrich, S. Piehler, C. Röcker, M. Rumpel, M. A. Ahmed, and T. Graf, in *Conference on Lasers and Electro-Optics*, OSA Technical Digest (2018), paper SM1N.4.
14. M. Zeyen, A. Antognini, K. Kirch, A. Knecht, M. Marszalek, F. Nez, J. Nuber, R. Pohl, I. Schulthess, and L. Sinkunaite, Proc. SPIE **10896**, 108960X (2019).
15. J. Neuhaus, J. Kleinbauer, A. Killi, S. Weiler, D. Sutter, and T. Dekorsy, Opt. Lett. **33**, 726 (2008).
16. J. Korner, J. Hein, H. Liebetrau, M. Kahle, F. Seifert, D. Kloepfel, and M. Kaluza, in *7th HEC-DPSSL Workshop* (2012).
17. T. Dietz, M. Jenne, D. Bauer, M. Scharun, D. Sutter, and A. Killi, Opt. Express **28**, 11415 (2020).
18. C. Herkommer, P. Krötz, R. Jung, S. Klingebiel, C. Wandt, R. Bessing, P. Walch, T. Produit, K. Michel, D. Bauer, R. Kienberger, and T. Metzger, Opt. Express **28**, 30164 (2020).
19. E. Perevezentsev, I. Kuznetsov, I. Mukhin, and O. V. Palashov, Appl. Opt. **56**, 8471 (2017).

https://doi.org/10.1017/hpl.2025.2 Published online by Cambridge University Press